Electronic and vibrational properties of nickel sulfides from first principles

Jeng-Han Wang, Zhe Cheng, Jean-Luc Brédas, and Meilin Liu

Citation: J. Chem. Phys. **127**, 214705 (2007); doi: 10.1063/1.2801985
View online: http://dx.doi.org/10.1063/1.2801985
View Table of Contents: http://jcp.aip.org/resource/1/JCPSA6/v127/i21
Published by the American Institute of Physics.

Additional information on J. Chem. Phys.

Journal Homepage: http://jcp.aip.org/
Journal Information: http://jcp.aip.org/about/about_the_journal
Top downloads: http://jcp.aip.org/features/most_downloaded
Information for Authors: http://jcp.aip.org/authors

ADVERTISEMENT

Downloaded 03 Apr 2013 to 130.207.50.154. This article is copyrighted as indicated in the abstract. Reuse of AIP content is subject to the terms at: http://jcp.aip.org/about/rights_and_permissions

Electronic and vibrational properties of nickel sulfides from first principles

Jeng-Han Wang
School of Materials Science and Engineering, Georgia Institute of Technology, Atlanta, Georgia 30332-0245, USA and School of Chemistry and Biochemistry, Georgia Institute of Technology, Atlanta, Georgia 30332-0400, USA

Zhe Cheng
School of Materials Science and Engineering, Georgia Institute of Technology, Atlanta, Georgia 30332-0245, USA

Jean-Luc Brédas[a),b)]
School of Chemistry and Biochemistry, Georgia Institute of Technology, Atlanta, Georgia 30332-0400, USA

Meilin Liu[a),c)]
School of Materials Science and Engineering, Georgia Institute of Technology, Atlanta, Georgia 30332-0245, USA

(Received 6 July 2007; accepted 2 October 2007; published online 6 December 2007)

We report the results of first-principles calculations (generalized gradient approximation–Perdew Wang 1991) on the electronic and vibrational properties of several nickel sulfides that are observed on Ni-based anodes in solid oxide fuel cells (SOFCs) upon exposure to H_2S contaminated fuels: heazlewoodite Ni_3S_2, millerite NiS, polydymite Ni_3S_4, and pyrite NiS_2. The optimized lattice parameters of these sulfides are within 1% of the values determined from x-ray diffraction. The electronic structure analysis indicates that all Ni–S bonds are strongly covalent. Furthermore, it is found that the nickel *d* orbitals shift downward in energy, whereas the sulfur *p* orbitals shift upward with increasing sulfur content; this is consistent with the decrease in conductivity and catalytic activity of sulfur-contaminated Ni-based electrodes (or degradation in SOFC performance). In addition, we systematically analyze the classifications of the vibrational modes at the Γ point from the crystal symmetry and calculate the corresponding vibrational frequencies from the optimized lattice constants. This information is vital to the identification with *in situ* vibrational spectroscopy of the nickel sulfides formed on Ni-based electrodes under the conditions for SOFC operation. Finally, the effect of thermal expansion on frequency calculations for the Ni_3S_2 system is also briefly examined. © *2007 American Institute of Physics*. [DOI: 10.1063/1.2801985]

I. INTRODUCTION

Nickel has been widely used as the anode for solid oxide fuel cells (SOFCs) because of its excellent catalytic ability for hydrogen oxidation, good electronic conductivity, and low cost. Upon exposure to sulfur-contaminated fuels, however, the performance of a Ni-based anode degrades rapidly, due likely to the adsorption of sulfur and/or formation of sulfides on Ni surfaces.[1–7] Nickel sulfide compounds present several stoichiometries, which are stable under different thermodynamic conditions; in addition, in the presence of O_2, the sulfur atoms can be quickly replaced by O atoms to form nickel oxide. Thus, nickel sulfides display a complex behavior and more detailed and systematic studies are required to understand their properties.

Experimental work[8–19] has shown that four nickel sulfides have relatively higher stability than other forms, including heazlewoodite Ni_3S_2, millerite NiS, polydymite Ni_3S_4, and pyrite NiS_2 (from nickel rich to sulfur rich). The structures of these sulfides have been thoroughly examined with x-ray diffraction (XRD): Ni_3S_2 has a stable rhombohedral structure,[8–10] NiS a hexagonal structure,[11–13] and Ni_3S_4 (Refs. 14–17) and NiS_2 cubic structures.[14,17–19] However, the vibrational spectra of the Ni-rich sulfides have not yet been clearly identified. Ni_3S_2, prepared from the impregnated thiosalt decomposition method and identified from the XRD pattern, shows no Raman active lines upon excitation at 514.5 nm from an Ar-ion laser.[20] In contrast, Bishop *et al.*[21] examined standard Ni_3S_2 (supplied from Aldrich) and found ten Raman peaks in the range of 140–438 cm^{-1} with a similar spectroscopic setup. In the NiS case, Shen *et al.*[22] observed five Raman peaks below 400 cm^{-1} in synthesized NiS nanorods. However, Bishop *et al.*[21] distinguished eight Raman peaks in the same range with a highly purified NiS powder (from Johnson Matthey GmbH). The Raman spectra of the S-rich compounds of Ni_3S_4 and NiS_2 have been reported in a more consistent way in previous studies.[21,23–27] The interpretation of the Raman spectra thus requires a more detailed characterization of the vibrational properties of these compounds; this is important in order to directly identify nickel sulfides on the Ni-based anode surface under SOFC operating conditions using *in situ* Raman spectroscopy,

[a)]Authors to whom correspondence should be addressed.
[b)]Electronic mail: jean-luc.bredas@chemistry.gatech.edu.
[c)]Electronic mail: meilin.liu@mse.gatech.edu.

 © 2007 American Institute of Physics

Downloaded 03 Apr 2013 to 130.207.50.154. This article is copyrighted as indicated in the abstract. Reuse of AIP content is subject to the terms at: http://jcp.aip.org/about/rights_and_permissions

which is vital to a fundamental understanding of the S-poisoning mechanisms.

The crystal structures and electronic band structures of the nickel sulfides have been widely studied by first-principles calculations.[15,28–34] The crystal structures are found to be accurately predicted from the calculations. The results of electronic and band structure calculations indicate that the Ni–S bonds in NiS and NiS_2 correspond to the interaction between sulfur *p* and nickel *d* orbitals and that the 3*d* metal sulfides of nickel have lower metal-sulfur bond strengths than the 4*d* metal sulfides, such as NbS, NbS_2, MoS_2, PdS, or RuS_2.[29] This weaker bond strength is responsible for the poorer catalytic activity of nickel sulfides, according to the interpretation of Norskov *et al.*[35] Furthermore, the variation in catalytic activities can also be understood from the band structure results[28,33,34] of Ni_3S_2 and NiS.

In the present work, the bulk properties of several important nickel sulfides have been systematically studied by first-principles calculations. Our goal is to better understand the impact of nickel sulfide formation on the irreversible sulfur poisoning in SOFCs. In addition, the crystal phonon modes of the sulfides have been characterized in terms of both symmetries and frequencies. Our results provide useful information for future nickel sulfide related research as they can be applied to identify the vibrational peaks and the nature of nickel sulfides via spectroscopic experiments.

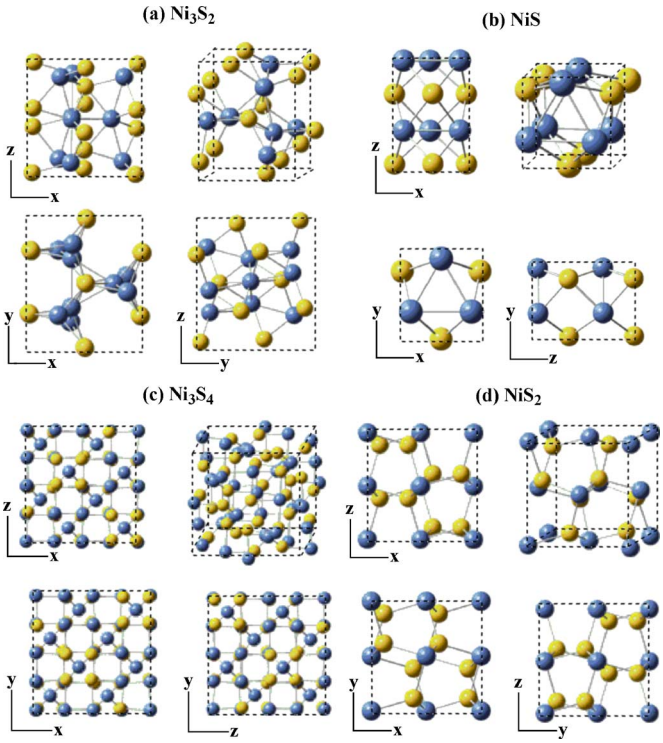

FIG. 1. (Color online) Crystal structures of Ni_3S_2, NiS, Ni_3S_4, and NiS_2 from different perspectives. Blue and yellow balls are represented as Ni and S atoms, respectively.

II. COMPUTATIONAL METHODOLOGY

The calculations have been carried out with the Vienna *ab initio* simulation package[36–38] (VASP) at the density functional theory (DFT) level with 3D periodic conditions.

A. Electronic structure calculations

We use the generalized gradient approximation[39] (GGA) with the Perdew-Wang 1991 (PW91) exchange-correlation functional[40] for the electronic structure calculations. The Kohn-Sham equations are solved on the basis of plane waves with kinetic energy below the chosen cutoff energy, 400 eV, and nonlocal optimized ultrasoft pseudopotentials. The Brillouin-zone (BZ) integration is sampled at about 0.05 $\times 2\pi(1/\text{Å})$ intervals in reciprocal space by the Monkhorst-Pack scheme.[41] Higher *k*-point values with smaller BZ sampling intervals, $<0.04\times 2\pi(1/\text{Å})$, are set to examine the convergence of current calculations. For example, lattice constants of NiS_2 of the *k* points as $4\times 4\times 4$ and $5\times 5\times 5$ along the $(100)\times(010)\times(001)$ directions in the supercell with four $[NiS_2]$ units have rather small difference, <0.01 Å. The cutoff energy and *k* points are determined so as to ensure convergence of the whole system and the efficiency of the computational procedure.

The crystal structures of the interest nickel sulfides, Ni_3S_2, NiS, Ni_3S_4, and NiS_2, are initially optimized and compared with XRD observations to validate the computational methodology. Based on the optimized structure, the charge distribution can be obtained by Bader charge analysis.[42–44] We note that in spite of some numerical differences between this and other charge analyses (e.g., the Mulliken charge analysis), these charge analyses provide qualitatively similar results. The atom-projected density of states (DOS) calculations for the sulfur *p* and nickel *d* orbitals are performed with Wigner-Seitz radii of $R(\text{Ni})=1.286$ Å and $R(\text{S})=1.164$ Å.

B. Vibrational analysis

The crystal phonons are computed from the optimized geometries by applying the finite displacement approach.[45,46] The interatomic force-constant matrix (Hessian matrix) is derived from a set of calculations on a periodically repeated supercell that contains several unit cells. At the starting point, all atoms are placed at the equilibrium position. Then each atom is slightly displaced and the forces on all atoms are calculated. These computed forces are proportional to the interatomic force constant times the displacement. By considering all symmetry-inequivalent displacements, the full Hessian matrix can be obtained. The Hessian matrix is truncated due to the finite size of the supercell; however, it rapidly decays to zero with increasing interatomic separations. The frequencies as a function of the normal modes are obtained via matrix diagonalization and are computed at the Γ point of the Brillouin zone in order to allow comparison with the spectroscopic data.

III. RESULTS AND DISCUSSION

A. Bulk properties of nickel sulfides

The crystal structures of Ni_3S_2, NiS, Ni_3S_4, and NiS_2 are illustrated in Fig. 1. In Fig. 1(a), heazlewoodite Ni_3S_2 has a rhombohedral (nearly cubic) structure, where S atoms form a

Downloaded 03 Apr 2013 to 130.207.50.154. This article is copyrighted as indicated in the abstract. Reuse of AIP content is subject to the terms at: http://jcp.aip.org/about/rights_and_permissions

TABLE I. The crystal parameters, internal atomic distances, and angles of Ni_3S_2, NiS, Ni_3S_4, and NiS_2 in the units of Å and deg.

	Computational results	Experimental results
	Ni_3S_2 (healzlewoodite, $R32$)[a]	
(a,γ)	(4.09, 89.4)	(4.08, 89.5);[b] (4.07, 89.5);[c] (4.06, 89.6)[d]
Ni–S	(2.26, 2.29)	(2.27, 2.27);[b] (2.25, 2.29)[d]
Ni–Ni	(2.51, 2.55)	(2.52, 2.52);[b] (2.50, 2.53)[d]
S–S	(3.55, 4.09)	(3.50, 4.08);[b] (3.51, 4.07)[d]
<S–Ni–S	(100.7, 127.7)	(100.7, 127.8);[b] (100.8, 127.3)[d]
<Ni–Ni–Ni	(60.0, 98.9, 108.0, 149.0)	(60.0, 99.2, 108.6, 147.9);[b] (60.0, 99.0, 108.1, 148.7)[d]
<Ni–S–Ni	(114.9, 127.7)	(112.6, 127.8);[b] (114.5, 127.3)[d]
	NiS (millerite, $R3m$)	
(a,c)	(9.62, 3.15)	(9.62, 3.15);[e] (9.59, 3.17);[f] (9.61, 3.14)[g]
Ni–S	(2.26, 2.38)	(2.26, 2.38);[e] (2.26, 2.37)[g]
Ni–Ni	2.55	2.53;[e] 2.53[g]
S–S	3.22	3.15;[e] 3.14[g]
<S–Ni–S	(85.3, 90.6, 95.8, 111.1)	(85.4, 91.6, 95.7, 110.6);[e] (85.4, 91.2, 95.6, 111.8)[g]
<Ni–Ni–Ni	60.0	60.0;[e] 60.0[g]
	Ni_3S_4 (polydymite, $Fd3m$)	
a	9.49	9.48;[h] 9.49;[i] 9.46;[j] 9.41[k]
	NiS_2 (pyrite, $Pa3$)	
a	5.69	5.69;[h]5.67;[k] 5.68;[l] 5.62[m]
Ni–S	2.40	2.39[l]
S–S	2.08	2.07[l]
S–Ni–S	93.5	93.5[l]
S–S–Ni	104.3	104.6[l]

[a]Nickel sulfide composition (crystal structure, space group).
[b]Reference 8.
[c]Reference 9.
[d]Reference 10.
[e]Reference 11.
[f]Reference 12.
[g]Reference 13.
[h]Reference 14.
[i]Reference 15.
[j]Reference 16.
[k]Reference 17.
[l]Reference 18.
[m]Reference 19.

slightly distorted body-centered cubic array with Ni atoms occupying the distorted tetrahedral interstices (a series of triangular bipyramids with three Ni atoms forming the triangle and two S atoms at the apex positions). In Fig. 1(b), millerite NiS has a hexagonal structure, where three Ni atoms form a triangle and five S atoms locate in the corners of a square pyramid. In Fig. 1(c), polydymite Ni_3S_4 has two types of Ni atoms and one type of S atoms, $Ni^{I}Ni^{II}_2S_4$, in a cubic structure. The Ni^{I} atom occupies 1/8 of the tetrahedral site, the two Ni^{II} atoms occupy half of the octahedral sites, which present a trigonal distortion along the (111) direction, and the four S atoms are on an approximate close-packed face-centered-cubic lattice. In Fig. 1(d), pyrite NiS_2 has a cubic structure, where the Ni atoms occupy the sites in the face-centered-cubic sublattice. The centers of the sulfur dimers (oriented along the (111) direction in the cubic cell) locate midway between the cubic edges and body center.

The crystal parameters, internal atomic distances, and angles of Ni_3S_2, NiS, Ni_3S_4, and NiS_2 are optimized and compared to the results of previous XRD works,[8–19] as listed in Table I. The agreement between the optimized lattice parameters and the experimental data is within 1%, the typical deviation of the GGA-PW91 method. We can thus be confident that our computational methodology is reliable to describe nickel sulfides. We now turn to a discussion of the Bader charge analyses and of the DOS calculations.

Listed in Table II is the Bader charge analyses of the nickel sulfides based on the optimized crystal structures. The Bader charges of Ni become more positive and those of S become less negative in sulfur-richer compounds; their range

TABLE II. Bader charges of Ni_3S_2, NiS, Ni_3S_4, and NiS_2.

Ni(3)		S(2)
	Ni_3S_2	
0.41		−0.62
	NiS	
Ni(1)		S(1)
0.48		−0.48
	Ni_3S_4	
Ni(1)	Ni(2)	S(4)
0.54	0.62	−0.45
	NiS_2	
Ni(1)		S(2)
0.60		−0.30

Downloaded 03 Apr 2013 to 130.207.50.154. This article is copyrighted as indicated in the abstract. Reuse of AIP content is subject to the terms at: http://jcp.aip.org/about/rights_and_permissions

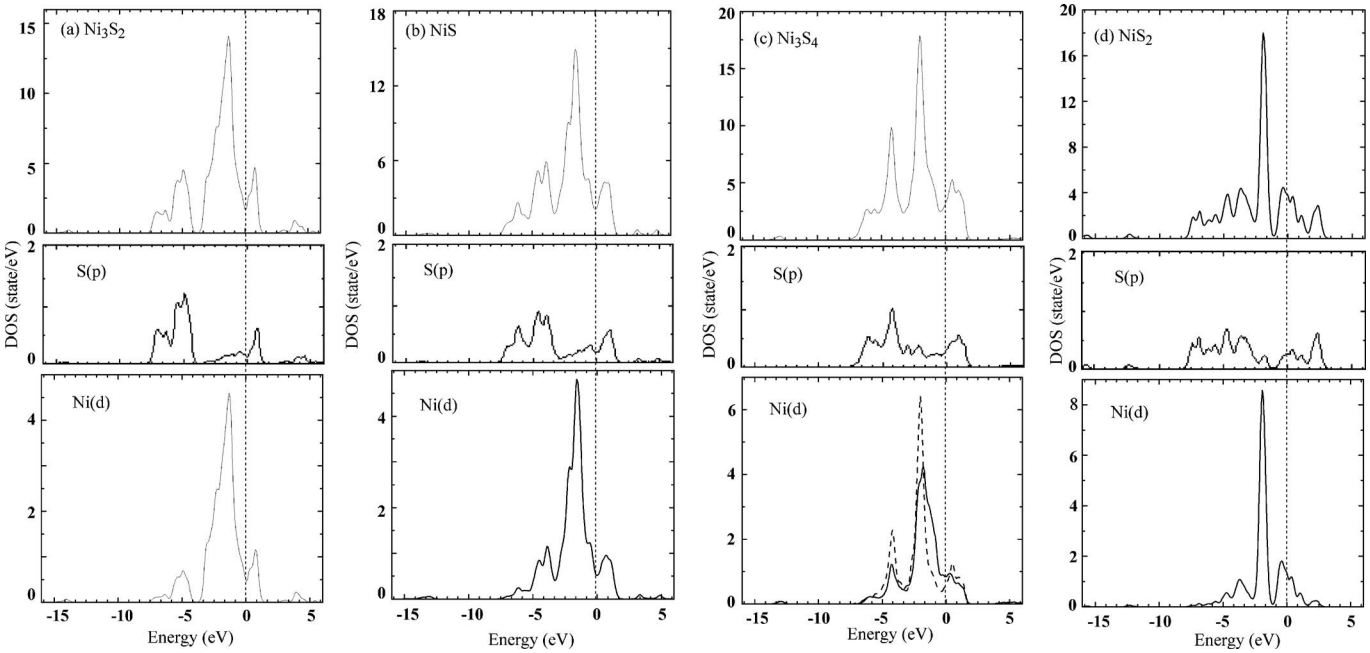

FIG. 2. DOS analysis for (a) Ni_3S_2, (b) NiS, (c) Ni_3S_4, and (d) NiS_2. The total and partial DOS of sulfur *p* and nickel *d* orbitals are shown in the top, middle, and bottom figures, respectively). The solid and dashed lines in Ni(d) of Ni_3S_4 represent the two types of Ni^{I} and Ni^{II} atoms, respectively.

for Ni is 0.41–0.62 $|e|$ and for S is −0.60 to −0.30 $|e|$. Compared with the Bader charges of the ionic NiO, Ni=1.22 $|e|$ and O=−1.22 $|e|$, the Ni–S bonds of these four compounds are significantly covalent.

Shown in Fig. 2 is the total DOS of Ni_3S_2, NiS, Ni_3S_4, and NiS_2 (top ones) and their partial sulfur *p* and nickel *d* orbitals (middle and bottom ones, respectively). The four nickel sulfides have very similar DOS distributions, in which nickel *d* orbitals present a large density below the Fermi level (valence band), while sulfur *p* orbitals contribute most above the Fermi level (conduction band). This result demonstrates the covalent interactions in these nickel sulfide compounds and is consistent with the outcome from the Bader charge analysis. In addition, the DOS of Ni_3S_2, NiS, and Ni_3S_4 are relatively low at the Fermi level. This result indicates that the crystal structures of these compounds are fairly stable since the stability of metal sulfides or alloys are typically corresponding to a low DOS at the Fermi level, as explained in previous works.[28,47–50] The computed DOS of NiS_2 shows a metallic behavior with the Femi level within the nickel *d* band. This band structure is similar to other pyrite-type sulfides of CoS_2 and ZnS_2 with high filling *d* band metals.[34,51]

As can be seen from the comparison of DOS for the four nickel sulfides shown in Fig. 3, the nickel *d*-band centers become more negative (down shifting away from the Fermi level), whereas the sulfur *p*-band centers become more positive (up shifting away from Fermi level) as the ratio of S to Ni increases. Because of the band gaps between nickel *d* band and sulfur *p* band, nickel sulfides are less conductive than pure Ni. Further, the down shifting of the *d* band centers of the nickel sulfides increases the reaction barriers to H_2 oxidization, leading to diminished catalytic activity toward fuel oxidation.[52] Thus, the degradation in performance of a Ni-based anode in a SOFC upon exposure to a

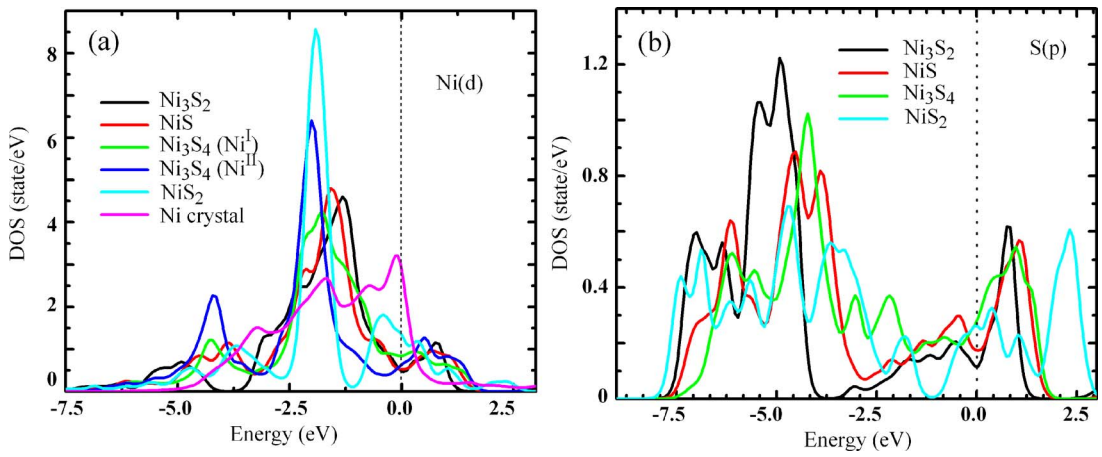

FIG. 3. (Color online) Comparison of the partial DOS for the (a) nickel *d* orbitals and (b) sulfur *p* orbitals.

Downloaded 03 Apr 2013 to 130.207.50.154. This article is copyrighted as indicated in the abstract. Reuse of AIP content is subject to the terms at: http://jcp.aip.org/about/rights_and_permissions

TABLE III. The classification of Ni_3S_2, NiS, Ni_3S_4, and NiS_2 crystal vibrations at the Γ point.

	Ni_3S_2	NiS	Ni_3S_4	NiS_2
Formula units	1	3	2	4
Dimension representations	15	18	42	36
Irreducible representations	$2A_1+3A_2+5E$	$4A_1+2A_2+6E$	$A_{1g}+E_g+F_{1g}+3F_{2g}$ $+2A_{2u}+2E_u+5F_{1u}+2F_{2u}$	$A_g+E_g+3F_g$ $+2A_u+2E_u+6F_u$
Raman active modes	$2A_1+4E$	$3A_1+5E$	$A_{1g}+E_g+3F_{2g}$	$A_g+E_g+3F_g$
IR active modes	$2A_2+4E$	$3A_1+5E$	$4F_{1u}$	F_u
Translations	A_2+E	A_1+E	F_{1u}	F_u

S-contaminated fuel is attributed to lower conductivity and poorer catalytic activity of the nickel sulfides than those of pure Ni.

B. Crystal vibrations at the Γ point

The Γ-point vibrational frequencies of the nickel sulfides have been calculated from the optimized crystal structures. The vibrational modes are classified as IR active, Raman active, or silent based on their crystal symmetries.[53] The classifications of the Ni_3S_2, NiS, Ni_3S_4, and NiS_2 crystal vibrations at the Γ point are summarized in Table III. The vibrational mode analysis from the crystal structures (Figs. 4–7) provides more detailed information about the crystal phonons. According to the classifications in Table III and the symmetries of the vibrational modes in Figs. 4–7, the computed Raman frequencies are assigned and compared with the Raman spectroscopic data as summarized in Table IV. These results are important to identify various nickel sulfides in spectroscopic experiments.

The heazlewoodite Ni_3S_2 crystal (space group: $R32$) consists of one formula unit, $[Ni_3S_2]$, in the unit cell and has 15-dimensional representations. The phonon modes at the Γ point can be classified according to symmetry as

$$\Gamma(Ni_3S_2) = 2A_1 + 3A_2 + 5E.$$

From the selection rules, the three translational modes A_2+E are silent; six modes are Raman active, $2A_1+4E$ and six modes are IR active, $2A_2+4E$. The six Raman-active modes in the primitive cell are shown in Fig. 4 together with their symmetry and frequencies. Our computational results are very useful to clarify the disagreement between the previous experimental observations[20,21] and helpful to identify the spectrum in our *in situ* sulfur-poisoning experiments.[27] The differences between calculated and observed frequencies are smaller than 20 cm^{-1}.

In the NiS crystal (space group: $R3m$), the unit cell has three formula units, $[NiS]_3$ and generates 18-dimensional representations at the Γ point.

$$\Gamma(NiS) = 4A_1 + 2A_2 + 6E.$$

From the selection rules, A_1+E correspond to the translations; the two A_2 modes are neither IR nor Raman active modes and the other modes ($3A_1$ and $5E$) are both IR and Raman modes. The vibrational frequencies and modes of these eight IR and Raman active modes are shown in Fig. 5.

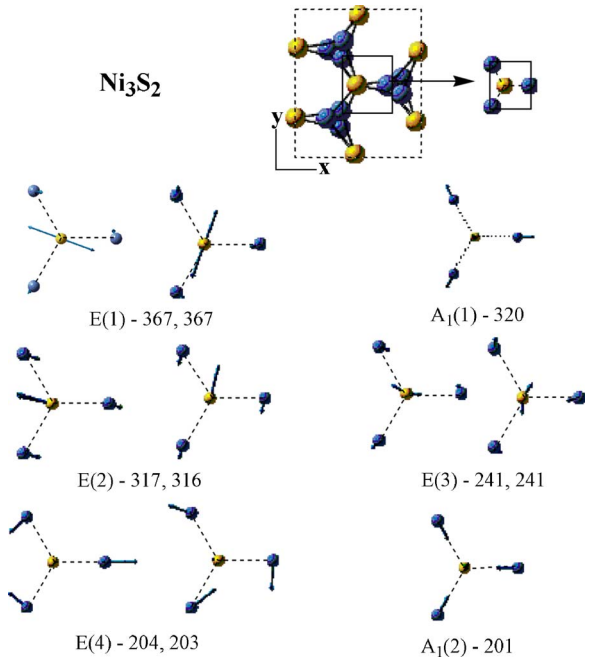

FIG. 4. (Color online) Ni_3S_2: vibrational mode analysis and related frequencies (cm^{-1}) of the primitive cell. Blue and yellow balls represent Ni and S atoms, respectively.

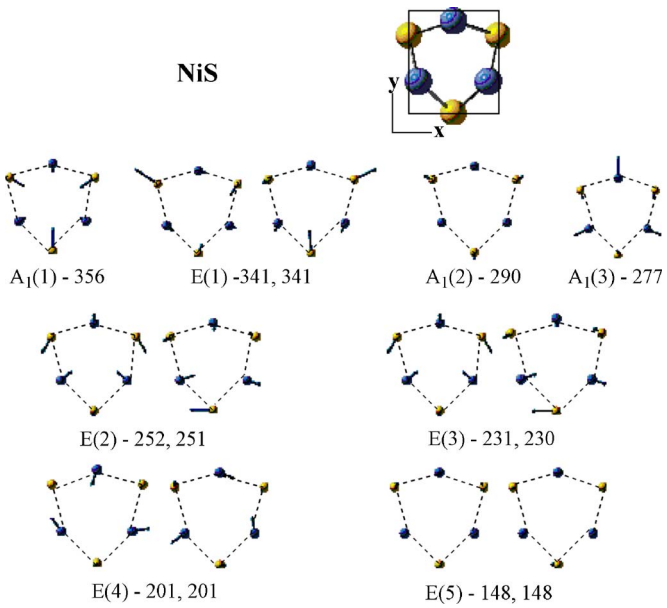

FIG. 5. (Color online) NiS: vibrational mode analysis and related frequencies (cm^{-1}) of the primitive cell. Blue and yellow balls represent Ni and S atoms, respectively.

Downloaded 03 Apr 2013 to 130.207.50.154. This article is copyrighted as indicated in the abstract. Reuse of AIP content is subject to the terms at: http://jcp.aip.org/about/rights_and_permissions

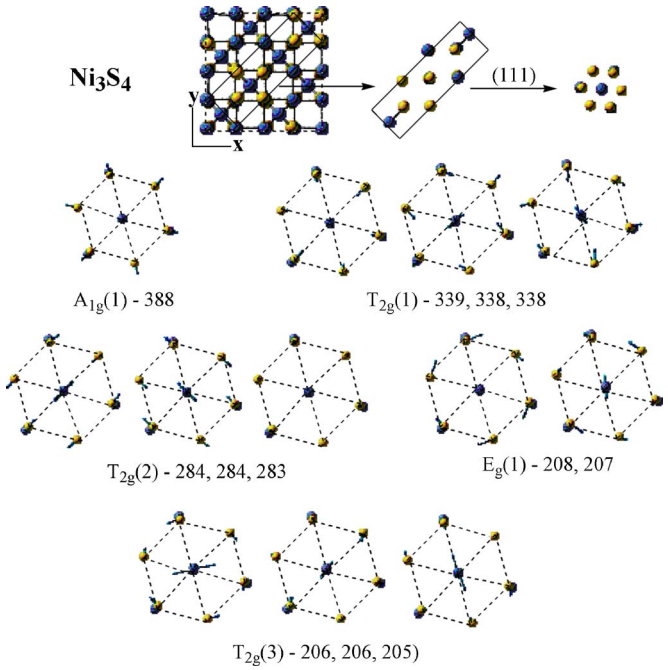

FIG. 6. (Color online) Ni_3S_4: vibrational mode analysis and related frequencies (cm^{-1}) of the primitive cell. Blue and yellow balls represent Ni and S atoms, respectively.

The computed vibrational frequencies also clarify the difference in the previous experiments[21–23] and present good agreement with the our spectroscopic results.[27] In addition, the $A_1(3)$ and $E(2)$ modes are too close to be distinguished in the Raman spectra but can be well separated in the calculations.

In the polydymite Ni_3S_4 crystal (space group: $Fd3m$), the unit cell has two formula units, $[Ni_3S_4]_2$ and results in

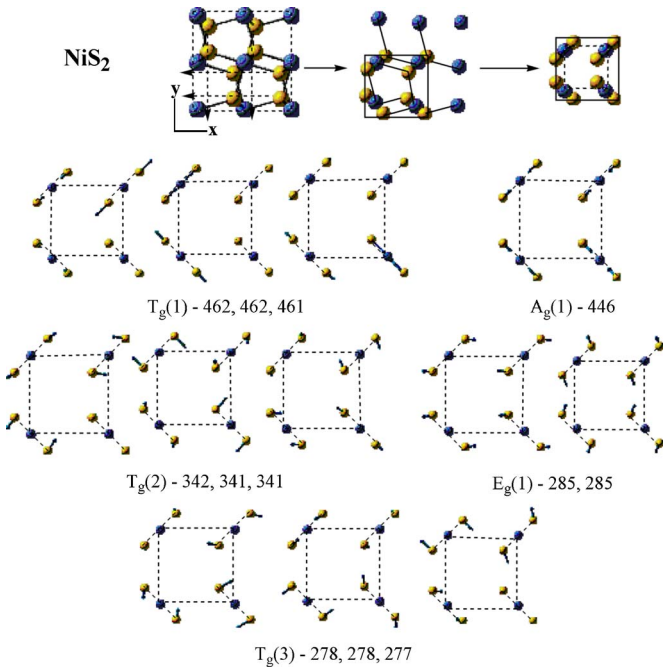

FIG. 7. (Color online) NiS_2: vibrational mode analysis and related frequencies (cm^{-1}) of the primitive cell. Blue and yellow balls represent Ni and S atoms, respectively.

total of 42-dimensional representations at the Γ point. The irreducible representations can be expressed as

$$\Gamma(Ni_3S_4) = A_{1g} + E_g + T_{1g} + 3T_{2g} + 2A_{2u} + 2E_u + 5F_{1u} + 2F_{2u}.$$

From the selection rules, one of the *ungerade* $2F_{2u}$ modes is related to the translations, four of the ungerade $5F_{1u}$ modes correspond to the IR-active modes, and the *gerade* symmetries of A_{1g}, E_g, and $3T_{2g}$ are attributed to the Raman-active modes. The five Raman modes of the primitive cell are represented in Fig. 6 shown from (111) perspective. The computed vibrational frequencies show good agreement with experiments.[23,27]

Finally, the $Pa3$ unit cell of NiS_2 crystal has four formula units, $[NiS_2]_4$ with 36-dimensional representations at the Γ point. The irreducible representations can be given as

$$\Gamma(NiS_2) = A_g + E_g + 3F_g + 2A_u + 2E_u + 6F_u.$$

From the selection rules, the three translational modes correspond to one of the F_u modes, the three IR active modes are related to ungerade F_u, and the five Raman active modes are found in gerade $A_g+E_g+3F_g$. The five Raman active modes and computed vibrational frequencies of the primitive cell of NiS_2 are represented in Fig. 7. The main difference between the computational and experimental works is the missing $T_g(2)$ mode in the Raman spectrum.[24–26] This difference could come from the coupling between the rotational and stretching vibrations of the S_2 dimer, as described for some other pyrite metal sulfides.[24,54,55] Each S_2 dimer itself has two degenerate rotational modes and one stretching mode. When the S_2 dimers occupy the four equivalent sites of the $Pa3$ structure, the stretching mode splits into $A_g(1)$ and $T_g(1)$ modes, and the two rotational modes split into $E_g(1)$, $T_g(2)$, and $T_g(3)$ modes. In the case of a weak rotation-stretching coupling [large frequency difference between $E_g(1)$ and $A_g(1)$ modes], the $A_g(1)$ mode has a frequency close to $T_g(1)$ mode, and $E_g(1)$ mode has a frequency close to $T_g(2)$ and $T_g(3)$ modes. On the other hand, the $T_g(2)$ frequency moves apart from that of $E_g(1)$ when the coupling gets stronger. In the current study, the computed coupling between $A_g(1)$ and $E_g(1)$ is slightly stronger than that in the experimental observations,[24–27] which pushes the $T_g(2)$ mode further away from the $E_g(1)$ mode. Therefore, the appearance of a separate $T_g(2)$ peak in the computational study might be the result of too strong a calculated coupling.

It is noted that the differences between the computed vibrational frequencies and the values measured with Raman spectroscopy for the four nickel sulfides are less than 10%, due probably to the effect of thermal expansion of the lattice and to the presence of lattice defects. At higher temperatures (e.g., under SOFC operating conditions), lattice expansion leads to longer bond lengths and lower vibrational frequencies. This effect can be estimated from the experimentally determined thermal expansion coefficients. For example, the thermal expansion coefficient of Ni_3S_2 is given by[10]

$$\alpha(T) = \alpha_0 + 7.286 \times 10^{-5} \times T$$

Downloaded 03 Apr 2013 to 130.207.50.154. This article is copyrighted as indicated in the abstract. Reuse of AIP content is subject to the terms at: http://jcp.aip.org/about/rights_and_permissions

TABLE IV. Calculated and experimentally observed Raman frequencies (cm^{-1}) of Ni_3S_2, NiS, Ni_3S_4, and NiS_2.

Ni_3S_2												
Modes	$E(1)$		$A_1(1)$	$E(2)$		$E(3)$		$E(4)$		$A_1(2)$		
Calc.	367	367	320	317	316	241	241	204	203	201		
Ref. 27	351		324	305		223		201		190		
NiS												
Modes	$A_1(1)$	$E(1)$		$A_1(2)$	$A_1(3)$	$E(2)$		$E(3)$		$E(4)$		$E(5)$
Calc.	356	341	341	290	277	252	251	231	230	201	201	148 148
Ref. 21	372	350		301	283	246		222		181		142
Ref. 22	369	349		300	283	244						144
Ref. 23	376	355		305		251		239		204		154
Ref. 27	370	349		300		246						
Ni_3S_4												
Modes	$A_{1g}(1)$	$T_{2g}(1)$				$T_{2g}(2)$		$E_g(1)$		$T_{2g}(3)$		
Calc.	388	339	338	338	284	284	283	208	207	206	206	205
Ref. 23	383		338			288		224		208		
Ref. 27	375		335			285		222				
NiS_2												
Modes	$T_g(1)$		$A_g(1)$			$T_g(2)$		$E_g(1)$		$T_g(3)$		
Calc.	462	462	461	446	342	341	341	285	285	278	278	277
Ref. 24		490		480				285			274	
Ref. 25		488		478							281	
Ref. 26		487		480				285			272	

$$\gamma(T) = \gamma_0 + 275.46 \times T.$$

We can use this equation to correct the lattice parameters of α_0=4.089 Å and γ_0=89.38 for Raman frequency calculations at high temperatures, as listed in Table V. The deviations of the computed frequencies at 300, 600, and 900 K from the experimentally determined values (Raman spectra) are reduced to less than 5.5%. Further, various structural and chemical defects present in the samples used for Raman measurements may also be partially responsible for the difference between computational and experimental results. The effect of lattice defects may influence not only the peak positions but also the vibrational modes; it is rather complicated and is still under investigation.

IV. CONCLUSIONS

The structural, electronic, and vibrational properties of several nickel sulfides relevant to sulfur poisoning of Ni-based anodes in a SOFCs, Ni_3S_2, NiS, Ni_3S_4, and NiS_2 have been examined using first-principles calculations. The lattice parameters of these nickel sulfides optimized at the (periodic) DFT level with GGA-PW91 method showed good agreement with XRD results. Analysis of the total and partial DOS, together with the Bader charges analysis, shows that Ni–S bonds are highly covalent and the down shifting of the *d* band centers of the nickel sulfides make sulfur-contaminated Ni electrodes less active toward hydrogen fuel oxidation. The vibrational modes and frequencies of the nickel sulfides at the Γ point have been systematically computed, which can be used for identification of these sulfide phases using Raman spectroscopy.

ACKNOWLEDGMENTS

This work was supported by the US Department of Energy (DOE) Solid State Energy Conversion Alliance (SECA) Core Technology Program (Grant No. DE-FC26-04NT42219), DOE Office of Basic Energy Sciences, Catalysis Science Program (Grant No. DE-FG02-06ER15837), and by the National Science Foundation (NSF) under the Chemistry Research Instrumentation and Facilities (CRIF) Award CHE-0443564. It was performed using the Molecular Science Computing Facility (MSCF) in Environmental Molecular Sciences Laboratory (EMSL), a national scientific user

TABLE V. Calculated Raman frequencies (cm^{-1}) of Ni_3S_2 before and after thermal expansion correction.

Modes	$E(1)$		$A_1(1)$	$E(2)$		$E(3)$		$E(4)$		$A_1(2)$
Uncorrected, 0 K	367	367	320	317	316	241	241	204	203	201
300 K	366	366	319	314	314	234	234	204	204	202
600 K	360	360	321	308	308	228	228	206	206	201
900 K	359	359	320	300	300	222	222	204	204	196

Downloaded 03 Apr 2013 to 130.207.50.154. This article is copyrighted as indicated in the abstract. Reuse of AIP content is subject to the terms at: http://jcp.aip.org/about/rights_and_permissions

facility sponsored by the U.S. DOE Office of Biological and Environmental Research (DOE/OBER) and located at Pacific Northwestern National Laboratory (PNNL).

[1] C. H. Bartholomew, P. K. Agrawal, and J. R. Katzer, Adv. Catal. **31**, 135 (1982).
[2] J. Dong, Z. Cheng, S. Zha, and M. Liu, J. Power Sources **156**, 461 (2006).
[3] A. I. Marquez, Y. De Abreu, and G. G. Botte, Electrochem. Solid-State Lett. **9**, A163 (2006).
[4] A. Burke, J. Winnick, C. Xia, and M. Liu, J. Electrochem. Soc. **149**, D160 (2002).
[5] S. Zha, Z. Cheng, and M. Liu, J. Electrochem. Soc. **154**, B201 (2007).
[6] Z. Cheng, S. Zha, and M. Liu, J. Electrochem. Soc. **153**, A1302 (2006).
[7] L. Aguilar, S. Zha, S. Li, J. Winnick, and M. Liu, Electrochem. Solid-State Lett. **7**, A324 (2004).
[8] M. E. Fleet, Am. Mineral. **62**, 341 (1977).
[9] J. B. Parise, Acta Crystallogr., Sect. B: Struct. Crystallogr. Cryst. Chem. **B36**, 1179 (1980).
[10] A. D. Vershinin, E. N. Selivanov, R. I. Gulyaeva, and N. I. Sel'menskikh, Inorg. Mater. **41**, 882 (2005).
[11] V. Rajamani and C. T. Prewitt, Can. Mineral. **12**, 253 (1974).
[12] N. H. Kolkmeijer and T. A. l. Moesvelt, Z. Kristallogr., Kristallgeom., Kristallphys., Kristallchem. **80**, 91 (1931).
[13] J. D. Grice and R. B. Ferguson, Can. Mineral. **12**, 248 (1974).
[14] K. Schubert, Acta Crystallogr., Sect. B: Struct. Crystallogr. Cryst. Chem. **B33**, 2631 (1997).
[15] D. J. Vaughan and J. R. Craig, Am. Mineral. **70**, 1036 (1985).
[16] D. Lundqvist, Ark. Kemi, Mineral. Geol. **24**, 1 (1947).
[17] L. G. Berry and R. M. Thompson, Mem.-Geol. Soc. Am. **85**, 78 (1962).
[18] E. Nowack, D. Schwarzenbach, and T. Hahn, Acta Crystallogr., Sect. B: Struct. Sci. **B47**, 650 (1991).
[19] T. Fujii, K. Tanaka, F. Marumo, and Y. Noda, Mineral. J. **13**, 448 (1987).
[20] U. S. Ozkan, L. Zhang, S. Ni, and E. Moctezuma, Energy Fuels **8**, 830 (1994).
[21] D. W. Bishop, P. S. Thomas, and A. S. Ray, Mater. Res. Bull. **35**, 1123 (2000).
[22] G. Shen, D. Chen, K. Tang, C. An, Q. Yang, and Y. Qian, J. Solid State Chem. **173**, 227 (2003).
[23] J. W. Anthony, R. A. Bideaux, K. W. Bladh, and M. C. Nichols, *Handbook of Mineralogy* (Mineral Data Publishing, Tucson, Arizona, 1990).
[24] C. de las Heras and F. Agullo-Rueda, J. Phys.: Condens. Matter **12**, 5317 (2000).
[25] P. Anastassakis, J. Chem. Phys. **64**, 3604 (1976).
[26] T. Suzuki, K. Uchinokura, T. Sekine, and E. Matsuura, Solid State Commun. **23**, 847 (1977).
[27] Z. Cheng and M. Liu, Solid State Ionics **178**, 925 (2007).
[28] Z. W. Lu, B. M. Klein, and D. J. Singh, Phys. Rev. B **54**, 13542 (1996).
[29] P. Raybaud, G. Kresse, J. Hafner, and H. Toulhoat, J. Phys.: Condens. Matter **9**, 11085 (1997).
[30] L. Koutti and J. Hugel, J. Phys.: Condens. Matter **11**, 1979 (1999).
[31] R. V. Kasowski, Phys. Rev. B **8**, 1378 (1973).
[32] G. V. Gibbs, R. T. Downs, C. T. Prewitt, K. M. Rosso, N. L. Ross, and D. F. Cox, J. Phys. Chem. B **109**, 21788 (2005).
[33] D. J. Vaughan and A. Tossel, Phys. Chem. Miner. **9**, 253 (1983).
[34] P. Raybaud, J. Hafner, G. Kresse, and H. Toulhoat, J. Phys.: Condens. Matter **9**, 11107 (1997).
[35] J. K. Norskov, B. S. Clausen, and H. Topsoe, Catal. Lett. **13**, 1 (1992).
[36] G. Kresse and J. Furthmüller, Phys. Rev. B **54**, 11169 (1996).
[37] G. Kresse and J. Furthmüller, Comput. Mater. Sci. **6**, 15 (1996).
[38] G. Kresse and J. Hafner, Phys. Rev. B **47**, 558 (1993).
[39] C. Lee, W. Yang, and R. G. Parr, Phys. Rev. B **37**, 785 (1988).
[40] J. P. Perdew and Y. Wang, J. Chem. Phys. **45**, 13244 (1992).
[41] H. J. Monkhorst and J. D. Pack, Phys. Rev. B **13**, 5188 (1976).
[42] R. W. F. Bader, *A Quantum Theory* (Oxford University Press, Oxford, 1990).
[43] G. Henkelman, A. Arnaldsson, and H. Jónsson, Comput. Mater. Sci. **36**, 254 (2006).
[44] E. Sanville, S. D. Kenny, R. Smith, and G. Henkelman, J. Comput. Chem. **28**, 899 (2007).
[45] X. Gonze, Phys. Rev. B **55**, 10337 (1997).
[46] G. Kresse, J. Furthmuller, and J. Hafner, Europhys. Lett. **32**, 729 (1995).
[47] Z. W. Lu, B. M. Klein, and A. Zunger, Phys. Rev. Lett. **75**, 1320 (1995).
[48] N. F. Mott and H. Jones, *The Theory of the Properties of Matels and Alloys* (Clarendon, Oxford, 1936).
[49] D. M. Nicholson, MRS Symposia Proceedings No. 133 (Materials Research Society, Pittsburg, 1989), p. 17.
[50] J.-H. Xu and A. J. Freeman, Phys. Rev. B **40**, 11927 (1989).
[51] A. Fujimori, K. Mamiya, T. Mizokawa, T. Miyadai, T. Sekiguchi, H. Takahashi, N. Môri, and S. Suga, Phys. Rev. B **54**, 16329 (1996).
[52] B. Hammer and J. K. Norskov, Adv. Catal. **45**, 71 (2000).
[53] J. R. Ferraro, K. Nakamoto, and C. W. Brown, *Introductory Raman Spectroscopy*, 2nd ed. (Academic, London, 2003).
[54] M. Blanchard, M. Alfredsson, J. Brodholt, G. D. Price, K. Wright, C. Richard, and A. Catlow, J. Phys. Chem. B **109**, 22067 (2005).
[55] C. Sourisseau, R. Cavagant, and M. Fouassier, J. Phys. Chem. Solids **52**, 537 (1991).

Downloaded 03 Apr 2013 to 130.207.50.154. This article is copyrighted as indicated in the abstract. Reuse of AIP content is subject to the terms at: http://jcp.aip.org/about/rights_and_permissions